JACS
JOURNAL OF THE AMERICAN CHEMICAL SOCIETY

Communication

pubs.acs.org/JACS

Mechanically Encoded Cellular Shapes for Synthesis of Anisotropic Mesoporous Particles

Kristin C. Meyer,[†] Eric N. Coker,[†] Dan S. Bolintineanu,[‡] and Bryan Kaehr*[,†,§]

[†]Advanced Materials Laboratory and [‡]Center for Integrated Nanotechnologies, Sandia National Laboratories, Albuquerque, New Mexico 87185, United States

[§]Department of Chemical and Biological Engineering, University of New Mexico, Albuquerque, New Mexico 87131, United States

Supporting Information

ABSTRACT: The asymmetry that pervades molecular mechanisms of living systems increasingly informs the aims of synthetic chemistry, particularly in the development of catalysts, particles, nanomaterials, and their assemblies. For particle synthesis, overcoming viscous forces to produce complex, nonspherical shapes is particularly challenging; a problem that is continuously solved in nature when observing dynamic biological entities such as cells. Here we bridge these dynamics to synthetic chemistry and show that the intrinsic asymmetric shapes of erythrocytes can be directed, captured, and translated into composites and inorganic particles using a process of nanoscale silica-bioreplication. We show that crucial aspects in particle design such as particle−particle interactions, pore size, and macromolecular accessibility can be tuned using cellular responses. The durability of resultant particles provides opportunities for shape-preserving transformations into metallic, semiconductive, and ferromagnetic particles and assemblies. The ability to use cellular responses as "structure directing agents" offers an unprecedented toolset to design colloidal-scale materials.

The success of living systems rests upon a mastery of molecular to microscale assemblies and materials. Multiscale processes such as metabolism, cell communication, and development rely on evolutionarily optimized structures to dictate function where the common thread of asymmetry pervades key aspects of these systems——from ligand receptor interactions to construction of hierarchical tissues. These principles increasingly inform synthetic chemistry and materials science; this is reflected, for instance, in recent aims of colloid chemistry where the development of asymmetric, anisotropic, patchy, Janus, and other nonspherical particles has gained substantial momentum and use across technological applications, materials engineering, and fundamental studies of self-assembly and recognition.[1] However, the development of nonspherical particles with prescribed shapes presents particular challenges given that bulk syntheses (e.g., solution or aerosol phase) of colloidal-scale materials tend to produce spherical particles due to the dominance of viscous and capillary forces (i.e., surface tension).[2a] This challenge, in part, has been overcome using a variety of strategies.[2] Despite these achievements, we still cannot synthetically mirror the complexity and precise control over shape observed in cells and microorganisms. This does not deter efforts but provides an inspirational pathway to achieve ever-higher complexity by developing foundational strategies from mimicking less elaborated shapes.

As an example, consider a mammalian erythrocyte (red blood cell, RBC). The characteristic biconcave discoid shape (termed a discocyte) provides excess surface area (40% compared to a sphere of the same volume) which ultimately gives rise to the majority of the mechanical and transport properties of RBCs by enabling extreme shape deformations.[3] These morphological and mechanical properties offer an explicit challenge for materials design and, as such, have been a target for efforts to synthesize particles that mimic RBC shapes and functions.[4] Given their lack of immune recognition and long circulation times, natural RBCs and their membrane components have been extensively investigated as therapeutic agents, but it is their extreme sensitivity to chemical and environmental changes——both of which are required for functionalization and/or drug loading——that has motivated efforts to improve durability by developing synthetic mimics and membrane/synthetic hybrid materials.[5] However, it is the concerted shape changes that RBCs undergo in response to chemical perturbation (Scheme 1a)——a response encoded mechanically in the membrane dynamics (Scheme 1b)[3,6]——which is intriguing to consider in the context of developing colloidal-scale nonspherical particles, that is, provided an ability to translate these shapes into more durable materials.

Here we systematically derive the RBC shape continuum (Scheme 1a) via perturbation of the RBC bilayer using crenating and cup-forming agents[7] (Scheme 1b) and translate these forms into composite and inorganic colloidal scale porous materials using a process of silica bioreplication (SBR; Scheme 1c).

To generate discocyte-shaped particles, purified RBCs were fixed prior to silicification (see Supporting Information [SI] for details). Cells were subsequently silicified in a saline solution at 40 °C containing 0.1 M silicic acid (derived from hydrolyzed tetramethyl orthosilicate, TMOS) adjusted to pH 3 for 12−18 h. Under these conditions (pH and silicic acid concentration) the solutions are highly stable[8−10] and display no gelation (self-condensation) over the course of weeks. Thus, silica deposition is limited to cellular surfaces——both internal and external——via a self-limiting mechanism that restricts silica layers to <10 nm[8]. To achieve a large proportion of discocytes, cells were used immediately in the above-described method. After the silica

Received: July 3, 2014
Published: August 29, 2014

   dx.doi.org/10.1021/ja506718z | J. Am. Chem. Soc. 2014, 136, 13138−13141

Scheme 1. (a) Schematic of the sequence of shapes displayed by RBCs. (b) These shape changes can be driven by chemical agents preferentially inserting into the inner (1) or outer (2) leaflet of the lipid bilayer to form cup or crenate shapes, respectively (adapted from ref 6). (c) Generation of a cup-shaped Si-RBC via silica bioreplication (SBR).

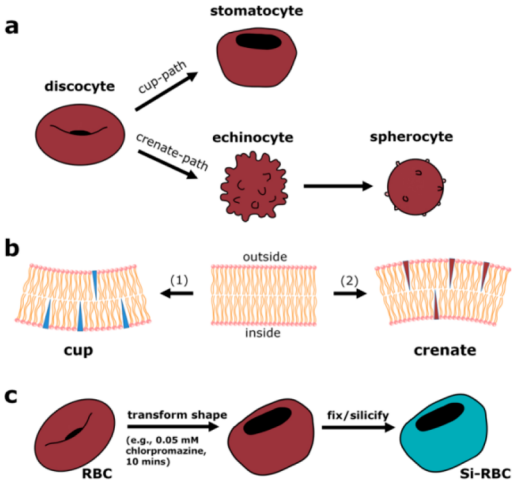

solution was rinsed, particles were dried in air from high vapor pressure solvents such as methanol and hexamethyldisilazane (HMDS).

Upon drying, we observed a uniform shrinkage of discocyte composite particles. Supporting Information, Figure S1 shows a single, flat-lying cell undergoing a change in diameter from 8.6 to 6.3 μm during drying. Assuming a normal cell volume of 90 fL, this decrease in diameter reduces the volume ~55% (~40 fL, assuming minimal change in discocyte height of ~1.5 μm). RBCs can display a wide range of cell volumes (20−200 fL) but cytoplasmic viscosity is tightly controlled by regulating hemoglobin concentration within a narrow range, and even minor (3−4%) changes in surface area can result in cell lysis.[3] This volume loss appears largely accommodated in composite discocytes by a compaction of the shape, resulting in a relatively pudgier morphology compared to normal, hydrated cells. SBR appears to impart mechanical stability to the cellular architecture during drying-induced stress; no cracking, lysing, or other morphological changes were observed.

Employing this general approach, we generated a range of silica composite particle libraries templated from the RBC shape sequence (Si-RBCs). The results are summarized in Figure 1a−d. Stomatocyte formation can be induced using cationic amphipaths, such as the antipsychotic drug chlorpromazine.[6] Echinocyte formation can be induced with anionic amphipaths, high salt, and ATP depletion which ultimately produces spherocytes, the most dense/compacted RBC shape.[11] Both stomatocyte and echinocyte formation involved relatively short treatments (≤10 min) prior to fixation; spherocyte particles were developed over longer treatment times (~24 h) using ATP depletion. Libraries with high yield of the target shapes were achieved for stomatocyte, discocyte, and spherocyte particles; however, synthesis of echinocytes using a range of chemical treatments consistently yielded a mixed population of both flattened (echinocyte I) and spikey (echinocyte II and III) crenated morphologies following drying (Figure 1a−c). The energy difference between these two forms is small[12] and increasing the concentration of crenating agents still yielded a significant fraction of the flattened echinocyte I shape.

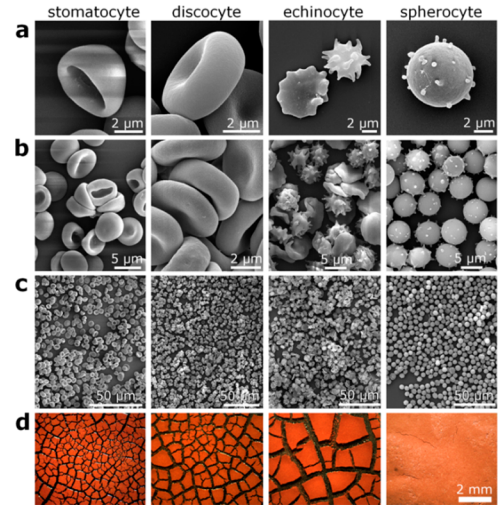

Figure 1. Generation of four distinct libraries of silica composite particles (Si-RBCs) templated from red blood cells. Panels a through c show decreasing magnification. (d) Panels show cracking patterns observed following drying in air from methanol.

Enrichment of echinocyte I and II populations potentially can be achieved using separations designed for nonspherical bioparticles.[13]

These libraries of distinctly shaped particles could be synthesized in scalable quantities. We found that approximately 4.5−5 mL of whole blood consistently yielded 1 g of dry dispersed particles (~10^{10} particles per gram). Silica replicas of Si-RBC shapes were obtained following calcination (550 °C, 4 h). Thermogravimetric analysis (TGA) showed that calcination to ~550 °C resulted in ~53% weight loss (Figure S2) from volatilization of the organic template accompanied by only minor shrinkage (~6% in diameter) and no discernible fracturing or change in shape compared to the starting material (Figure S3).

Next, we cast solutions comprising HMDS-dried particles (HMDS reacts with exposed silanols on the Si-RBCs to form terminal trimethylsilyl groups that increase the hydrophobicity of individual particles) dispersed in methanol and observed their properties as they assembled into films. Contact angle (θ) measurements of the resultant hydrophobic films showed increasing surface hydrophobicity as particle composition of the films progressed from stomatocyte/discocyte morphology to echinocytes and spherocytes. Films comprising the latter two presented a coarser, more hierarchical surface compared to stomatocyte/discocyte films and displayed superhydrophobicity ($\theta \approx 150°$; Figure S4).

Indeed depending on their differing shapes, single to few layers of particles were observed to combine into clusters (Figure 1b,c). As layers deposited and ultimately dried, we observed characteristic cracking patterns for each shape following rapid drying (Figure 1d). The formation of these patterns is controlled by a wide range of parameters, including drying rate as well as interparticle, capillary, and hydrodynamic forces. The salient differences among these structures can be explained by considering the variation in interparticle attraction/cohesion across particle libraries (evident, for instance, when comparing Figure 1 panels b and c). We have carried out Brownian dynamics-like simulations of particle drying on the scale of several particle layers, where the interparticle forces are modeled by varying the strength of a shifted Lennard-Jones potential (Figure S5, S6). In the case of spherocytes, where particles are

dx.doi.org/10.1021/ja506718z | J. Am. Chem. Soc. 2014, 136, 13138−13141

essentially spheres that present small protrusions, the attraction is relatively low; as a result, individual particles can rearrange freely with respect to one another to accommodate drying stresses, resulting in a surface free of cracks. At the opposite end are echinocytes which interlock into mechanically stable 3D clusters, ultimately forming the largest domains (Figure 1d). We model this with a larger interparticle attraction force, which results in the formation of larger clusters in the simulations. Despite the simple spherically symmetric interaction model, the simulations qualitatively reproduce the resulting particle microstructures (Figure S5). This indicates that particle aggregation on the scale of several particle layers may play a key role in the resulting cracking patterns.

These interesting properties provide opportunities to better understand and ultimately tune bulk systems based on jammed packing of hard, nonspherical particles, an area lacking well-defined experimental systems despite considerable theoretical work.[14] These packing characteristics could prove favorable over existing technologies for applications such as separations, filtration, and decontamination, and would be further enabled if Si-RBCs display suitable internal particle features such as well-defined porosity and high surface area. Previously we observed that calcined silica replicas of Chinese hamster ovarian (CHO) cells exhibited a wide range of meso- to macroscale pores.[8] This was expected given the complex interior of tissue-derived, nucleated cells. However, mammalian RBCs are anucleate, devoid of organelles, and consisting of a relatively homogeneous cytoplasm composed primarily of hemoglobin.

Thus, we examined the internal properties of individual particle libraries using physisorption. N_2 sorption isotherms obtained from calcined (500 °C, 4 h) particles are shown in Figure 2. Analysis of the sorption isotherms using nonlocal density functional theory (NLDFT) indicates a high surface area that is relatively consistent (~640−680 m^2/g) across the particle libraries. The isotherms obtained from discocyte and stomatocyte-templated silica particles show a similar sorption response (Figure 2a), indicating little change in mesopore composition as RBC-templated particles transition from native (discocyte) to cup (stomatocyte) morphology. However, as particles transform along the discoyte−echinocyte−spherocyte pathway, a comparison of the isotherms (Figure 2b) shows striking differences at higher partial pressures, with distinct hysteresis loops. These are indicative of differences in pore structure and connectivity but are difficult to precisely interpret.[15] NLDFT analysis of pore dimensions shows peak values of 4−6 nm across all samples (Figure 2c), which roughly corresponds to the average diameter of native hemoglobin.[16] However, an increase in larger mesopores is evident as particles progress from discocytes along the crenate pathway, eventually forming spherocytes. This indicates that changes in internal structure/organization following the addition of crenating agents are ultimately conferred to the silica replica. As cytoplasmic components aggregate or otherwise condense during crenation, their extraction via calcination results in larger pores, as evidenced by the largest pore sizes obtained from spherocyte replicas, templated from the RBCs with highest internal density.[11]

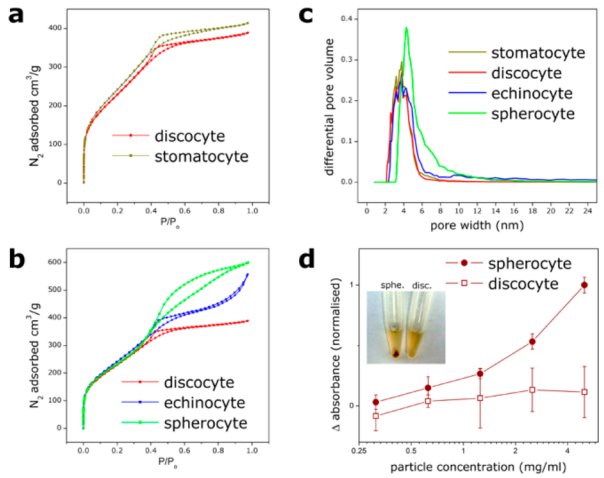

Figure 2. N_2 sorption isotherms of calcined Si-RBC particles from libraries in Figure 1 (panels a and b: the discocyte isotherm from panel a is duplicated in panel b for comparison) following removal of the cellular template via calcination (calcined Si-RBCs). (c) DFT pore size distribution calculated from the isotherms. (d) Differential loading of myoglobin into spherocytes versus discocytes as shown by normalized absorbance difference ($\Delta abs = [(A_0 - A_{30\ min})/A_0]$) of the supernatant following 30 min incubation (error bars indicate the standard deviation from triplicate measurements). The inset shows pelleted particles in myoglobin solution where loading is visible for spherocyte versus discocyte particles.

We speculated that these apparent differences in porosity conferred differences in macromolecular accessibility. To address this question, we incubated calcined discocytes and spherocytes in a solution of myoglobin (a ~3.5 nm diameter protein) and measured protein uptake using the 409 nm absorption peak of myoglobin. In contrast to discocytes, the protein visibly loaded into spherocyte silica particles (Figure 2d), indicating a more accessible pore network for the stomatocyte particles despite no apparent differences in pore structure as seen in TEM images of crushed silica particles (Figure S7). We estimate loading of ~10^8 myoglobins per spherocyte particle which, to put into perspective, is roughly an order of magnitude less heme content than a normal red blood cell (~10^9).

Lastly, locking induced cellular dynamics into a "Si-cell" provides a starting point for further shape-preserved transformations into other functional materials such as noble metals (e.g., Pt; Figure S8), semiconductors (e.g., Si; Figure S9), and magnetically-responsive particles (Figure 3a,b). Here, Si-cells

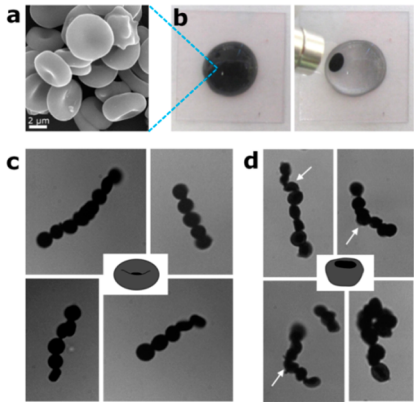

Figure 3. Magnetic Si-RBCs. (a) SEM of silica composite discocyte particles following iron infiltration and pyrolysis, which renders a solution of particles in water opaque (b, left panel) and responsive to a strong magnet (b, right panel). In the absence of an external magnetic field, particles self-assemble into linear (c, discocytes) or kinked (d, stomatocytes; arrows indicate kinking loci) chains depending on particle symmetry, which governs magnetic dipole−dipole interactions.

dx.doi.org/10.1021/ja506718z | J. Am. Chem. Soc. 2014, 136, 13138−13141

were pyrolyzed following iron ion infusion to generate weakly ferromagnetic particles (containing iron carbide; Figures S10, S11) that assemble into linear (Figure 3c) or kinked (Figure 3d) structures depending on the symmetry of the constituent particles. Similar materials transformations have been generously explored using silica templates;[17] applying the RBC shape continuum provides a new element of structural control that can enable studies examining effects of, for example, geometric curvature[18] and magnetic symmetry[19] for materials development and self-assembly.

Importantly, the replication of cellular structure in silica provides a chemical handle to silane chemistry, allowing nearly limitless opportunities for surface functionalization, for instance, to dictate selective dispersibility in organic and aqueous phases (Figure S12). This will prove enabling particularly if bioactivity can be maintained. Indeed, silicification does not appear to inhibit, for example, the peroxidase activity of RBCs (Figure S13). Maintenance of more delicate (e.g., O_2 and CO binding) and more complex (e.g., glycolysis) functions in Si-RBCs presents opportunities for future work that could enable development of general strategies to address challenges for biocatalyst stabilization.[20]

Given the accumulated wealth of information regarding how cells receive and respond to signals and coordinate behavior, this knowledge can now be reexamined as a starting point for the design of particles and materials. We have demonstrated this approach by exploiting the well-known morphological response of RBCs to chemical agents and have uncovered the potential to tune internal structure/porosity in a mesoporous material using a biological response. Similar internal templating can be considered in other soft cell templates, for instance, using GTP-activation to induce cytoskeletal rearrangements toward creation of hierarchical or unbranched networks.[21] Large internal pores could be developed using vacuole inducing agents.[22] Further functionalization, for example, with natural[23] or synthetic membranes[24] should facilitate *in vivo* applications. Overall, the addition of "cell diversity" and "differentiation" to the material synthesis toolkit offers an unprecedented pathway for further exploration.

■ ASSOCIATED CONTENT

Supporting Information

Detailed methods and Figures S1−S13. This material is available free of charge via the Internet at http://pubs.acs.org.

■ AUTHOR INFORMATION

Corresponding Author

bjkaehr@sandia.gov

Notes

The authors declare no competing financial interest.

■ ACKNOWLEDGMENTS

This work was supported by the U.S. Department of Energy, Office of Science, Basic Energy Sciences, Materials Sciences and Engineering Division. This work was performed, in part, at the Center for Integrated Nanotechnologies, a U.S. Department of Energy, Office of Basic Energy Sciences user facility. Sandia National Laboratories is a multiprogram laboratory managed and operated by Sandia Corporation, a wholly owned subsidiary of Lockheed Martin Corporation, for the U.S. Department of Energy's National Nuclear Security Administration under Contract No. DE-AC04-94AL85000. We thank Paul Durfee, Darren Dunphy, and Dale Huber for technical assistance.

■ REFERENCES

(1) (a) Walther, A.; Müller, A. H. *Chem. Rev.* **2013**, *113*, 5194. (b) Lee, K. J.; Yoon, J.; Lahann, J. *Curr. Opin. Colloid Interface Sci.* **2011**, *16*, 195. (c) Glotzer, S. C.; Solomon, M. J. *Nat. Mater.* **2007**, *6*, 557. (d) Helgeson, M. E.; Chapin, S. C.; Doyle, P. S. *Curr. Opin. Colloid Interface Sci.* **2011**, *16*, 106.

(2) (a) Shum, H. C.; Abate, A. R.; Lee, D.; Studart, A. R.; Wang, B.; Chen, C. H.; Thiele, J.; Shah, R. K.; Krummel, A.; Weitz, D. A. *Macromol. Rapid Commun.* **2010**, *31*, 108. (b) Yin, Y.; Lu, Y.; Gates, B.; Xia, Y. *J. Am. Chem. Soc.* **2001**, *123*, 8718. (c) Roh, K.-H.; Martin, D. C.; Lahann, J. *Nat. Mater.* **2005**, *4*, 759. (d) Dendukuri, D.; Pregibon, D. C.; Collins, J.; Hatton, T. A.; Doyle, P. S. *Nat. Mater.* **2006**, *5*, 365. (e) Merkel, T. J.; Herlihy, K. P.; Nunes, J.; Orgel, R. M.; Rolland, J. P.; DeSimone, J. M. *Langmuir* **2009**, *26*, 13086.

(3) Mohandas, N.; Gallagher, P. G. *Blood* **2008**, *112*, 3939.

(4) (a) Haghgooie, R.; Toner, M.; Doyle, P. S. *Macromol. Rapid Commun.* **2010**, *31*, 128. (b) Doshi, N.; Zahr, A. S.; Bhaskar, S.; Lahann, J.; Mitragotri, S. *Proc. Natl. Acad. Sci. U.S.A* **2009**, *106*, 21495. (c) Merkel, T. J.; Jones, S. W.; Herlihy, K. P.; Kersey, F. R.; Shields, A. R.; Napier, M.; Luft, J. C.; Wu, H.; Zamboni, W. C.; Wang, A. Z. *Proc. Natl. Acad. Sci. U.S.A.* **2011**, *108*, 586.

(5) Hu, C. M. J.; Fang, R. H.; Zhang, L. *Adv. Healthcare Mater.* **2012**, *1*, 537.

(6) Sheetz, M. P.; Singer, S. *Proc. Natl. Acad. Sci. U.S.A.* **1974**, *71*, 4457.

(7) Wong, P. *J. Theor. Biol.* **1999**, *196*, 343.

(8) Kaehr, B.; Townson, J. L.; Kalinich, R. M.; Awad, Y. H.; Swartzentruber, B. S.; Dunphy, D. R.; Brinker, C. J. *Proc. Natl. Acad. Sci. U.S.A.* **2012**, *109*, 17336.

(9) Khripin, C. Y.; Pristinski, D.; Dunphy, D. R.; Brinker, C. J.; Kaehr, B. *ACS Nano* **2011**, *5*, 1401.

(10) Iler, R. K. *The Chemistry of Silica*; Wiley: New York, 1979.

(11) Hoffman, R.; Benz Jr., E. J.; Silberstein, L. E.; Heslop, H.; Weitz, J.; Anastasi, J. *Hematology: Diagnosis and Treatment*; Elsevier Health Sciences: Philadelphia, PA, 2013.

(12) Wortis, M.; Mukhopadhyay, R. *Proc. Natl. Acad. Sci. U.S.A.* **2002**, *99*, 16766.

(13) Zeming, K. K.; Ranjan, S.; Zhang, Y. *Nat. Commun.* **2013**, *4*, 1625.

(14) Torquato, S.; Stillinger, F. H. *Rev. Mod. Phys.* **2010**, *82*, 2633.

(15) Pierotti, R.; Rouquerol, J. *Pure Appl. Chem.* **1985**, *57*, 603.

(16) Perutz, M. *Nature* **1948**, *161*, 204.

(17) (a) Sandhage, K. H.; Allan, S. M.; Dickerson, M. B.; Snyder, R. L. *Handbook of Biomineralization: Biomimetic and Bioinspired Chemistry*; Wiley-VCH: Weinheim, Germany, 2007; pp 2. (b) Losic, D.; Mitchell, J. G.; Voelcker, N. H. *Adv. Mater.* **2009**, *21*, 2947.

(18) Walker, D. A.; Leitsch, E. K.; Nap, R. J.; Szleifer, I.; Grzybowski, B. A. *Nat. Nanotechnol.* **2013**, *8*, 676.

(19) Yan, J.; Bloom, M.; Bae, S. C.; Luijten, E.; Granick, S. *Nature* **2012**, *491*, 578.

(20) (a) Stepankova, V.; Bidmanova, S.; Koudelakova, T.; Prokop, Z.; Chaloupkova, R.; Damborsky, J. *ACS Catal.* **2013**, *3*, 2823. (b) Hanefeld, U.; Gardossi, L.; Magner, E. *Chem. Soc. Rev.* **2008**, *38*, 453.

(21) Hall, A. *Science* **1998**, *279*, 509.

(22) Geng, Y.; Kohli, L.; Klocke, B. J.; Roth, K. A. *Neuro-oncology* **2010**, *12*, 473.

(23) Hu, C. M. J.; Zhang, L.; Aryal, S.; Cheung, C.; Fang, R. H.; Zhang, L. F. *Proc. Natl. Acad. Sci. U.S.A.* **2011**, *108*, 10980.

(24) Liu, J. W.; Stace-Naughton, A.; Jiang, X. M.; Brinker, C. J. *J. Am. Chem. Soc.* **2009**, *131*, 1354.